Pergamon

Int. J. Heat Mass Transfer. Vol. 37, No. 11, pp. 1545–1562, 1994

0017–9310/94 $7.00+0.00

0017–9310(94)00004–E

Marangoni–Bénard instability in microgravity conditions with Soret effect

A. BERGEON, D. HENRY and H. BENHADID

Ecole Centrale de Lyon/Université Claude Bernard-Lyon 1, Laboratoire de Mécanique des Fluides et d'Acoustique, URA CNRS 263, ECL-BP 163-69131 Ecully Cedex, France

(*Received* 19 *November* 1993 *and in final form* 18 *December* 1993)

Abstract—The Marangoni flows are studied by numerical simulation in a liquid layer with an undeformable free upper surface heated by a constant flux and with a rigid bottom at constant temperature. Multirolls structures with different symmetry properties are exhibited in the case of a one-component fluid. More insight is given to the situation with an aspect ratio $A = 4$ with the determination of bifurcations up to a time dependent flow. The focus of the study is on the influence of the Soret effect on the flow structure when the fluid is a non-reactive binary mixture. Stationary results are compared to the expected behaviour given by previous linear stability analyses. Situations where time dependent flows occur as first bifurcation are also computed: an interesting behaviour corresponding to the successive apparition of new rolls in the middle and on the sides of the cavity is obtained, for which a physical interpretation is proposed.

1. INTRODUCTION

OUR PURPOSE is to study the flow structures resulting from the Marangoni instability under a zero gravity level when the fluid is a one-component liquid or when it consists of a non-reactive binary mixture subjected to Soret effect. Such an instability may occur when a liquid material exhibits a free surface subjected to a surface tension effect. The variations of temperature and/or concentration along the free surface induce surface tension gradients which act as surface driven forces and tend to pull the fluid along the surface. We study the onset of convection in a rectangular cavity with a constant temperature imposed on the lower rigid boundary and a constant heat flux on the upper free surface. Above a critical temperature difference between the bottom and the top, the thermal and viscous dissipative processes are not sufficient to stop the fluid motion which arises, for example, from the natural temperature fluctuations along the free surface. Thus, above some critical values of the Marangoni number Ma_c, cellular patterns can be observed and are usually referred to as the Marangoni–Bénard instability. The critical Marangoni values of the first primary bifurcation to a steady state were first calculated analytically by Pearson [1] in the case of an infinite horizontal layer. Pearson's analysis is subjected to the assumptions that the interface is undeformable and that there are no buoyancy forces. The early study accounting for both buoyancy and surface tension effects on a fluid layer was performed by Nield [2]. Theoretical extensions of Nield's model have been conducted by Davis [3], Scanlon and Segel [4], Cloot and Lebon [5]. They particularly pointed out that for a sufficiently large Marangoni number, convection is possible even if there is a stabilizing effect of the gravity force (negative Rayleigh number). Large differences with the previous works have been observed in studying systems for which the surface deformation is permissible (Scriven and Sternling [6], Smith [7], Goussis and Kelly [8], Davis and Homsy [9], Castillo and Velarde [10]). Those works pointed out that, when the Marangoni number is less than a critical value, a deformable interface with a given capillary number leads to a stabilization compared to a plane interface.

Most of the previous developments are restricted to layers having an infinite horizontal extension. The effect of the lateral walls has been studied by means of non-linear analysis. The early analysis is due to Rosenblat *et al.* [11] who exhibited the pattern selection for different aspect ratios in a three-dimensional cavity. Particular attention is given to double bifurcation points for particular aspect ratios where two modes of different wavelengths compete. The authors also replace the 'no-slip' condition at the side walls by the idealized slippery condition. A comparison between these lateral boundary conditions in a two-dimensional cavity is carried out by Dijkstra [12, 13] who found that in comparison to 'slippery' conditions on the lateral walls, 'no-slip' conditions stabilize the system leading to a greater critical Marangoni number.

The study of Marangoni flows can also be performed in the case of a binary mixture subjected to Soret effect which is the diffusion of species under the effect of temperature gradients in addition to the classical species diffusion (Fick's law) [14]. Consequently, the concentration gradients are formed via the Soret effect in response to the applied thermal gradients rather than imposed externally by the boundary conditions. Performing a linear stability

NOMENCLATURE

A	aspect ratio, L/H
c	dimensionless mass fraction (concentration)
D	solutal diffusivity
D_S	phenomenological Soret coefficient
D_f	phenomenological Dufour coefficient
H	height of enclosure
J_q	heat flux
J_c	mass flux
k_c	dimensionless critical wave number
L	length of enclosure
Ma	Marangoni number
$\overline{Ma}$	modified Marangoni number
Pr	Prandtl number, ν/κ
q	algebraic heat flux applied on the free surface
S_M	dimensionless ratio of solutal to thermal contribution to the surface force
Sc	Schmidt number, ν/D
t	dimensionless time
T	dimensionless temperature
T^*	modified dimensionless temperature
u	dimensionless velocity component in the x direction
v	dimensionless velocity component in the z direction
x	dimensionless horizontal coordinate
X	modified dimensionless mass fraction
z	dimensionless vertical coordinate.

Greek symbols

γ_T, γ_c	partial derivative of surface tension, $\gamma_T = 1/\sigma_0 \cdot \partial\sigma/\partial T$, $\gamma_c = 1/\sigma_0 \cdot \partial\sigma/\partial c$
ζ	dimensionless vorticity
κ	thermal diffusivity
λ	thermal conductivity
λ_c	critical wavelength
μ	viscosity
ν	kinematic viscosity
ρ	density
σ	surface tension
ψ	streamfunction
ψ_M	modified dimensionless number S_M

analysis of the Rayleigh–Bénard convection in binary mixture with Soret effect, Knobloch [15] pointed out that such a problem is equivalent to the thermohaline convection studied by Nield [16] in the sense that there exists a linear transformation between one into the other. Extensions to realistic boundary problems were conducted by Hurle and Jakeman [17] and Knobloch and Moore [18]. There are few works dealing with Marangoni convection in Soret binary mixtures induced only by surface forces (i.e. under a zero gravity level). Castillo and Velarde [19] and Vaerenbergh *et al.* [20] performed a linear analysis in the situation of an infinite horizontal layer for which the interface is undeformable. They thus exhibited the expected wavelength for the first primary bifurcation and the corresponding critical value of the Marangoni number as a function of the ratio of solutal to thermal contribution to the surface force S_M. As for a particular choice of (Ma, S_M) the two contributions compete in an opposite way, oscillatory motions are predicted.

Our study is a contribution to emphasize the role of the Soret effect in thermocapillary driven convection under a zero gravity environment. For simplicity, we assume that the interface is undeformable. We restrict ourselves to a two-dimensional bounded cavity as it is known that two-dimensional roll patterns are those predicted for a three-dimensional rectangular cavity having the shorter side comparable to the depth and the longer side larger than the depth [11].

First of all, we consider a homogeneous liquid (pure thermal case). As the onset of convection is entirely controlled by the Marangoni number, particular attention is given to the influence of the Prandtl number and the aspect ratio of the cavity on the flow structure. The evolution with the Marangoni number is considered for a situation with an aspect ratio $A = 4$ with the determination of bifurcations up to a time dependent flow.

In a second part we consider a binary mixture and we introduce the thermal diffusion of species. Steady and time periodic flows are computed. For steady situations particular attention is given to the symmetry properties and the wavelength of the flows. Very interesting behaviours are obtained in situations where time dependent flows occur as first bifurcation.

2. FORMULATION

We consider a horizontal rectangular cavity with an aspect ratio $A = L/H$ (where L is the length and H the height of the cavity) filled with an incompressible Newtonian binary fluid mixture (Fig. 1). The upper

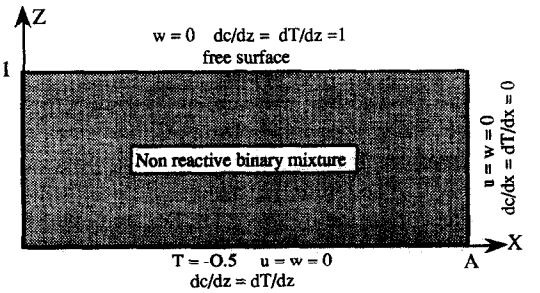

FIG. 1. Cavity configuration.

boundary is a plane free surface subjected to a constant normal heat flux q while the bottom boundary is a rigid wall maintained at a constant temperature T_0.

In microgravity conditions, there are no external forces and the onset of convection is due to surface tension which is supposed to vary linearly with mass fraction and temperature:

$$\sigma = \sigma_0(1+\gamma_T(T-T_0)+\gamma_c(c-c_0)) \qquad (1)$$

where γ_T and γ_c are constants:

$$\gamma_T = \frac{1}{\sigma_0}\left[\frac{\partial\sigma}{\partial T}\right]_{T_0,c_0} \gamma_c = \frac{1}{\sigma_0}\left[\frac{\partial\sigma}{\partial c}\right]_{T_0,c_0}. \qquad (2)$$

Considering a non reactive binary mixture, we use the general relations between the heat and mass flux and the thermodynamic forces [14]:

$$J_q = -\lambda\nabla T - \rho D_f \nabla c$$

$$J_c = -\rho D\nabla c - \rho D_S \nabla T \qquad (3a, b)$$

where λ is the thermal conductivity, D the mass diffusivity, D_s and D_f the phenomenological coefficients for the Soret and Dufour effects, respectively. We suppose all the coefficients to be constant in the range of temperature and concentration expected and we neglect the Dufour effect ($D_f = 0$). The problem is non-dimensionalized by using H^2/ν, H, ν/H, ΔT and Δc as scale quantities for time, length, velocity, temperature and concentration. $\Delta T = -qH/\lambda$ is the temperature difference resulting from the constant flux applied on the free surface when the diffusive state is well established. Δc is the concentration difference obtained at the Soret diffusive state as the result of the applied temperature difference, $\Delta c = -D_S{\cdot}\Delta T/D$. The dimensionless temperature and concentration are taken as $(T-T_m)/\Delta T$ and $(c-c_0)/\Delta c$, respectively, where c_0 is the initial mass fraction and $T_m = T_0+\Delta T/2$. The governing equations result from the conservation laws for an incompressible fluid and lead to the following nonlinear system in vorticity–streamfunction formulation:

$$\partial_t\zeta + (u\cdot\nabla)\zeta = \nabla^2\zeta$$

$$\zeta + \nabla^2\psi = 0$$

$$Pr\cdot(\partial_t T + (u\cdot\nabla)T) = \nabla^2 T$$

$$Sc\cdot(\partial_t c + (u\cdot\nabla)c) = \nabla^2 c - \nabla^2 T \qquad (4a, b, c, d)$$

valid in the domain $]0, A[\times]0,1[$ for $t \geqslant 0$, where $Pr = \nu/\kappa$ is the Prandtl number, $Sc = \nu/D$ the Schmidt number, ψ the streamfunction, $u = d\psi/dz$ and $w = -d\psi/dx$, respectively, the x (horizontal) and z (vertical) component of the velocity, ζ the y component of vorticity (normal to the cavity). The boundary conditions are 'no-slip' conditions on the rigid walls and insulating conditions on the two lateral boundaries. The normal mass flux is zero on the boundaries and a stress resulting from surface tension is applied on the free surface. We obtain the following system for the boundary conditions:

at $z = 0$:

$$T = -0.5, \quad \psi = u = w = 0, \quad \frac{\partial c}{\partial z} = \frac{\partial T}{\partial z}$$

at $z = 1$:

$$\psi = w = 0, \quad \frac{\partial c}{\partial z} = \frac{\partial T}{\partial z} = 1, \quad \frac{\partial u}{\partial z} = \frac{Ma}{Pr}\left(\frac{\partial T}{\partial x} + S_M\frac{\partial c}{\partial x}\right)$$

at $x = 0$ and $x = A$:

$$\psi = u = w = 0, \quad \frac{\partial c}{\partial x} = \frac{\partial T}{\partial x} = 0 \quad (5a, b, c)$$

where Ma is the Marangoni number and S_M the ratio of solutal to thermal contribution to the surface force:

$$Ma = \frac{\Delta T\cdot H\cdot\sigma_0\cdot\gamma_T}{\rho\cdot\nu\cdot\kappa}, \quad S_M = -\frac{D_S\cdot\gamma_c}{D\cdot\gamma_T}. \qquad (6)$$

Under the effect of the constant heat flux on the homogeneous mixture ($c(x,z) = c_0$), the concentration gradients build up until a final stationary state where the diffusion flux (equation (3b)) vanishes. Expressed in dimensionless form, the diffusive initial state is $u = w = 0$ and $T(z) = c(z) = z-0.5$.

As the diffusive state is always a solution of the equations, the onset of convection is obtained by perturbating the temperature gradient on the free surface with $\partial T/\partial x(x = x0,\ z = 1) = A'$. A weak roll is then created that will increase or decrease depending on the stability of the situation. The location and the sign of the perturbation will influence the configuration of the steady state: the sign of the quantity $Ma.\ A'$ indicates the direction of the surface force and thus the direction of the induced flow. The absolute amplitude A' (chosen between 0.02 and 2) has less importance: similar evolutions are obtained in all cases.

The problem is solved by using a Hermitian finite difference method with an alternative implicit direction scheme [21] in a grid of 61×21 points on (x,z) directions for the aspect ratio $A = 3$, 121×21 points for $A = 4$, 6 and 161×21 points for $A = 8$, 10. Two algorithms are used, steady or time dependent, according to the nature of the expected flow.

3. RESULTS FOR A ONE-COMPONENT FLUID

3.1. *Influence of the aspect ratio*

As it is established that 'no-slip' conditions on the lateral walls stabilize the system, the Marangoni number is taken equal to 100, above the critical value $Ma_c = 80$ calculated by Pearson [1] in the case of an infinite horizontal layer.

Numerical results are presented by the plot of streamlines and iso-values of the temperature for $Pr = 0.6$, $A = 3, 4, 8, 10$. Figure 2(a) shows the multiroll structure of the flow. As an entire number of rolls has to fit in the cavity, the mean wavelength (corresponding to two counter-rotating rolls) changes

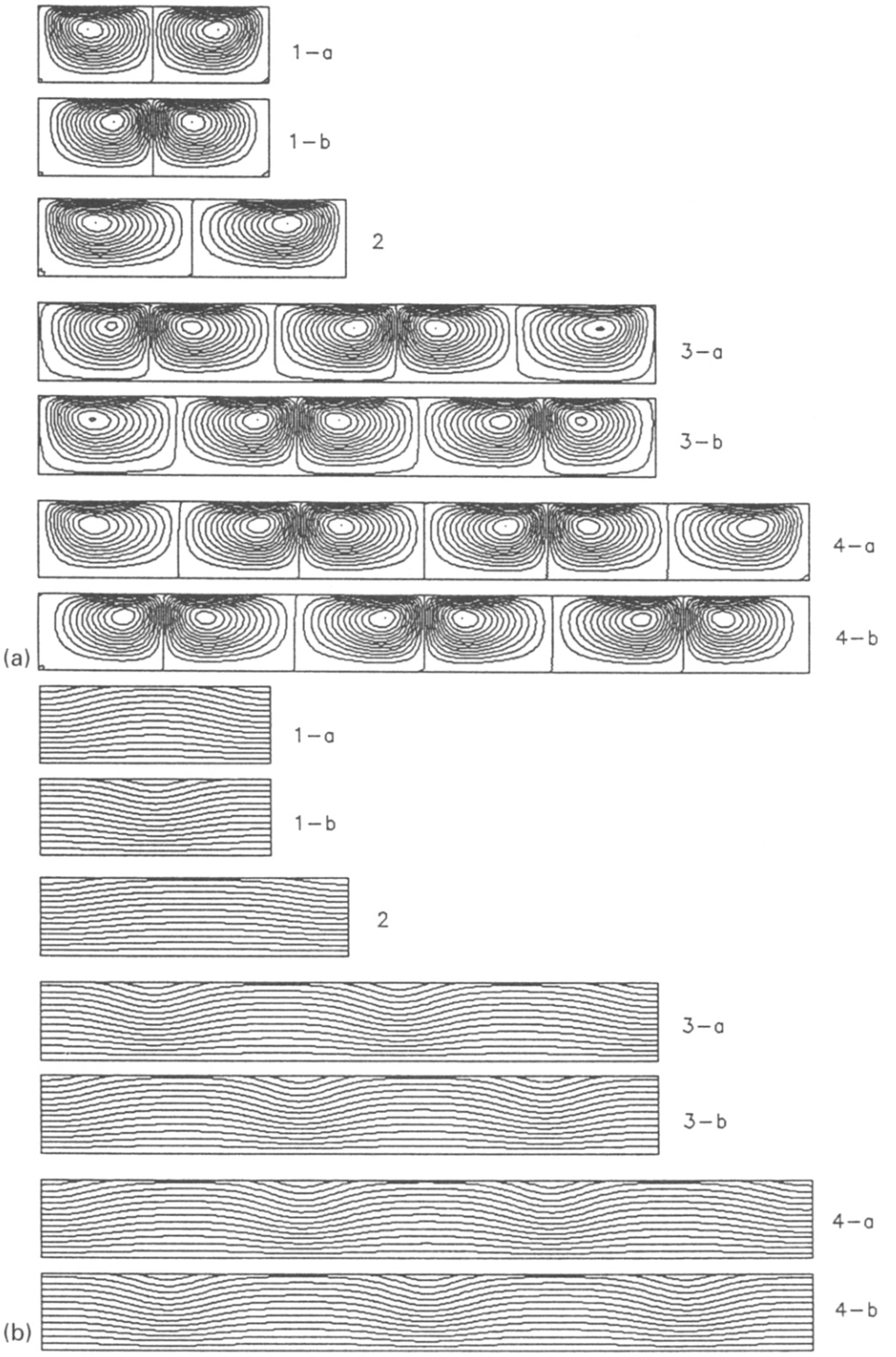

FIG. 2. Isovalues of the streamfunction (a): 25 isovalues between the minimum and the maximum indicated in Table 1, and isovalues of the temperature field (b): 20 isovalues between -0.5 and the maximum indicated in Table 1 and located on the free surface, for $Pr = 0.6$, $Ma = 100$ and (1) $A = 3$, (2) $A = 4$, (3) $A = 8$, (4) $A = 10$. Two solutions are obtained in the cases (1), (3), (4) by changing the sign of the perturbation A' (which is applied on the free surface to initiate the convective state): (a) $A' = +2$, (b) $A' = -2$.

Table 1. Mean wavelength of the flow structure, maximum (ψ_+) and minimum (ψ_-) of the streamfunction and maximum of the temperature field (T_{max}) as a function of the aspect ratio of the cavity. (a) and (b) refers to the two solutions obtained

Aspect ratio	Wavelength	ψ_-	ψ_+	T_{max}
3(a)	3.0	−0.7542	0.7542	0.5873
3(b)	3.0	−0.7073	0.7073	0.5891
4	4.0	−0.5219	0.5219	0.5728
8(a)	3.2	−0.8962	0.9057	0.6106
8(b)	3.2	−0.9057	0.8962	0.6106
10(a)	3.3	−0.9036	0.9037	0.6108
10(b)	3.3	−0.8578	0.8579	0.6113

when the aspect ratio is modified (Fig. 2). But the values are around the value obtained by Pearson [1] for an infinite layer: $\lambda_c \approx \pi$ ($k_c \approx 2$). Due to the surface tension drag along the interface, each roll is not symmetric: the flow is stronger in the zones where it goes downward. The deformations of the temperature field are induced by the flow (Fig. 2(b)). As the temperature is destabilizing, a deformation near the free surface in the direction of the vertical flow induces two opposite horizontal temperature gradients which generate two contrarotative rolls.

Due to the different boundary conditions between the bottom and the top, the only symmetry of the original problem is a vertical axi-symmetry S_Δ (reflection with respect to the vertical line $x = A/2$). For a given aspect ratio, two configurations with opposite senses of rotation of the cells can be expected. Effectively, by changing the sign of the initial perturbation A', two solutions have been obtained in the cases $A = 3$, 8, 10. For $A = 8$, an odd number of cells is obtained. Each of the two structures has lost the vertical symmetry but one is the image by the S_Δ-symmetry of the other (they are S_Δ-symmetry related, Fig. 2(a) (case 3)). For $A = 10$ and $A = 3$ an even number of cells is obtained (Fig. 2(a) (cases 1 and 4)). Each configuration is S_Δ-symmetric but they correspond to different structures (see values of ψ in Table 1). This is in good agreement with the assumption that the ensemble of possible solutions has to be invariant under the broken symmetry of the original problem. This symmetry requirement for the ensemble of possible bifurcated solutions constrains the form of the amplitude equation. Thus, the bifurcation to an even number of cells which does not break the vertical axi-symmetry S_Δ ($A = 3$, 10) is a transcritical one with two non-symmetry related branches: a subcritical branch which gives rise to an hysteresis and a supercritical one which is the less convective (for a given Ma). On the contrary, the bifurcation to an odd number of cells which breaks the S_Δ-symmetry property ($A = 8$) is a pitchfork bifurcation with two supercritical S_Δ-related branches. Winters *et al.* [22] discussed the symmetry properties of the bifurcation to convective flow in such Marangoni situations and Dijkstra [13] gave bifurcation diagrams (only the thermal condition at the upper boundary is slightly different). Their results are in good agreement with those presented here.

In the case $A = 4$, only the subcritical solution (two-cell pattern with centre upflow) is obtained. The supercritical solution with centre downflow is not obtained even if we force it by imposing a positive perturbation at the point $x = A/4$ on the free surface. The initial state evolves to a three-roll configuration before reaching the two-roll solution we have just described.

This particular behaviour at $A = 4$ is related to the vicinity of the transition between two and three rolls. In a 'slippery' model, the typical dimensionless wavelength of a two-roll configuration is around 3.1 for a Biot number equal to zero as in our situation [13] (the same value is obtained in an infinite layer [1]). As an entire number of rolls has to fit in the cavity, the two- and three-roll configurations compete for an aspect ratio around four. This situation looks similar to the one well pictured in Dijkstra's study [13] for an aspect ratio of three with $Bi = 20$ (Fig. 3). (For this value of Bi and in a 'no-slip' model, the typical dimensionless wavelength is about 2.4, which still gives for an aspect ratio of three, a competition between two- and three-roll configurations.) The first primary bifurcation is a pitchfork bifurcation to a three-roll structure and occurs for Ma_{13}. It gives rise to two unstable subcritical branches which coalesce giving a closed curve located below Ma_{13}. The second primary bifurcation is a transcritical bifurcation to a two-roll structure and occurs for $Ma_{12} > Ma_{13}$. As the trivial branch is one time unstable for $Ma_{13} < Ma < Ma_{12}$, the supercritical branch is one time unstable and the subcritical branch is two times unstable. The subcritical branch intersects the closed curve for Ma_{22} through a pitchfork bifurcation and becomes stable after a saddle node point. Thus, only one stable two-roll configuration with centre upflow can be obtained which corresponds to the subcritical branch. This is what we obtain for an aspect ratio $A = 4$ and a Biot number $Bi = 0$. The difference of aspect ratio with our situ-

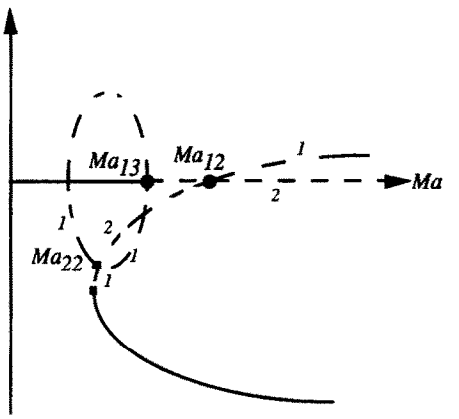

FIG. 3. Possible sketch of the bifurcation for an aspect ratio $A = 4$ (ref. [13]). On the vertical axis is plotted the velocity at a given point of the cavity.

ation is compensated by the changes with the Biot number which affect the characteristics of the neutral mode.

3.2. *Influence of the Prandtl number*

It can be proved by writing the linear perturbation equations with a choice of dimensionless time and velocity in H^2/κ and κ/H, respectively, that the critical Marangoni number of the first primary bifurcation to a steady state does not depend on the Prandtl number. Increasing the Prandtl number from $Pr = 0.6$ to 10 in the case $A = 4$, $Ma = 100$ does not change the structure of the flow but leads to a diminution of the flow intensity expressed in v/H units. Figure 4 shows the evolution of the temperature and velocity on the free surface in six situations with different Prandtl numbers ranging from 0.6 to 10. The maximum of the temperature field is located on the lateral boundary on the free surface and the minimum of the free surface, in the middle of the cavity. It can be noted that the maximum of temperature difference and the temperature gradient on the free surface increase with the Prandtl number whereas the maximum velocity decreases (see also Fig. 5). This could be a contradiction but the effect of the Prandtl number $(1/Pr)$ in the free boundary condition (equation (5b)) restores the contribution of the temperature gradient to the surface force: du/dz, which represents the surface force, is a decreasing quantity with the Prandtl number. The plot of the maximum velocity as a function of the maximum temperature difference is pictured in Fig. 5. In the range of the Prandtl number from 0.6 to 10, a linear evolution is established with a decrease of V_{max} in $Pr^{-0.9}$ (Fig. 5).

3.3. *Influence of the Marangoni number for an aspect ratio $A = 4$ and $Pr = 0.6$*

For a Marangoni number equal to 110 the system loses the S_Δ-symmetry. Two S_Δ-symmetry related stable solutions resulting from a pitchfork bifurcation from the previous steady state are obtained (Fig. 6). For a Marangoni number greater than 115 these branches bifurcate to an oscillatory motion through a Hopf bifurcation. The Hopf characteristic is given by the fact that, for a Marangoni number lower than 115, steady solutions are the result of a damped oscillatory motion with a constant period (for a given Marangoni number). Thus, the steady solutions bifurcate with a finite period that decreases with the increase of the Marangoni number. The flow structure has been computed for $Ma = 150$ and is presented through a period $T = 1.5$ (viscous time) in Figs. 7 and 8. As it can be seen, a quasi-constant roll is always present on the right of the cavity. In the left part, there is an evolution between one and three rolls. The two-roll situation at $t = 0$ with centre upflow presents a stronger and larger left roll. The onset of the perturbation that leads to the appearance of two additional contrarotative rolls between the two previous ones is induced by a perturbation of the temperature field on the free surface, located near the middle of the cavity in the weakly convective right part of the left roll. The evolution of the temperature profile on the free surface described in Figs. 9(a) and (b) shows the amplification of this perturbation and its characteristic of left-travelling wave, which leads to the swelling of the right new roll until it reaches the left boundary.

4. RESULTS FOR A TWO-COMPONENT FLUID WITH SORET EFFECT

4.1. *Preliminary remarks*

The boundary condition on the free surface can be regarded as the sum of two surface forces acting on the fluid motion:

$$\frac{\partial u}{\partial z} = f_{surface} = f_T + f_c \tag{7}$$

where f_T is the thermal contribution and f_c the mass fraction defined as:

$$f_T = \frac{Ma}{Pr}\frac{\partial T}{\partial x} \quad f_c = \frac{Ma}{Pr} S_M \frac{\partial c}{\partial x}. \tag{8}$$

Ma and S_M, previously defined, are algebraic quantities as the applied temperature difference ΔT and the quantities γ_T, γ_c can be positive or negative. Considering the diffusive state, suppose that a fraction of fluid is moved up from the bottom to the top of the cavity. Temperature and concentration gradients are thus created and induce two contributions to the surface force. As the boundary conditions for T and c are different, four situations have to be considered [19]: (a) $Ma < 0$, $S_M > 0$: the two contributions tend to oppose the movement. The situation is stable and no convection can occur. (b) $Ma > 0$, $S_M < 0$: only the solutal contribution has a stabilizing effect and time dependent flows are predicted by the linear stability analysis [19]. (c) $Ma < 0$, $S_M < 0$ and (d) $Ma > 0$, $S_M > 0$: in those cases, the linear stability analysis for an infinite horizontal layer predicts that the system bifurcates to a steady state.

The dimensionless parameters which control the onset of convection for a steady state can be obtained in a more general form than the one used in the literature by using the following change of variable:

$$X = \frac{1}{Sc}(c - T) \quad T^* = \frac{1}{Pr}T. \tag{9}$$

The linearized equations lead (for a steady state) to the following system:

$$\begin{aligned} \nabla p - \nabla^2 v &= 0 \\ w &= \nabla^2 T^* \\ w &= \nabla^2 X \\ \nabla \cdot v &= 0 \end{aligned} \tag{10}$$

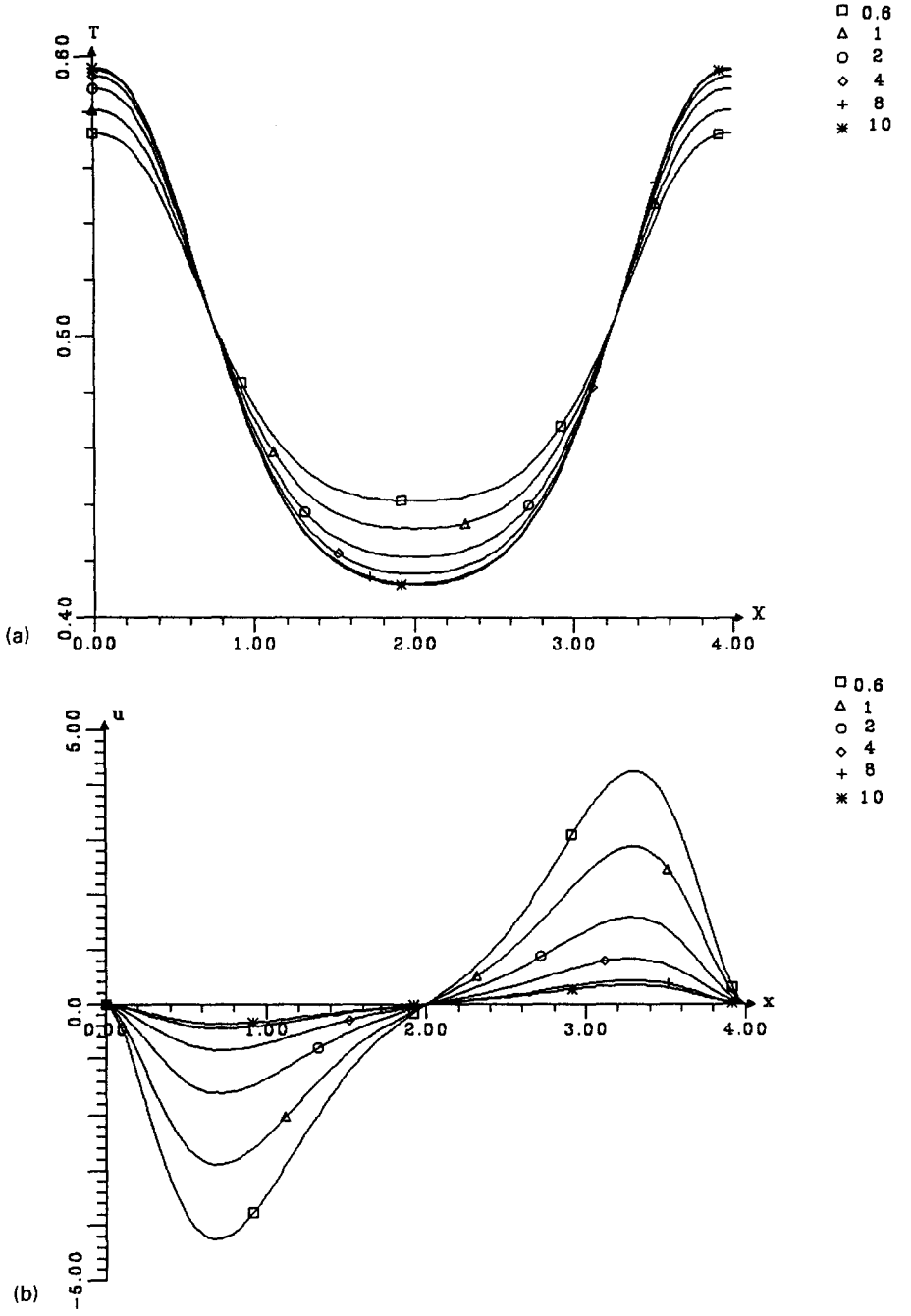

FIG. 4. Temperature (a) and velocity (b) on the free surface as a function of the Prandtl number indicated close to the labels ($A = 4$ and $Ma = 100$).

where v (u, w), p, T^*, X are the perturbations of the diffusive state. The boundary conditions become:

at $x = 0$ and $x = A$

$$\frac{\partial X}{\partial x} = \frac{\partial T^*}{\partial x} = u = w = 0$$

at $z = 0$

$$\frac{\partial X}{\partial z} = T^* = u = w = 0$$

at $z = 1$

$$\frac{\partial X}{\partial z} = \frac{\partial T^*}{\partial z} = w = 0. \qquad (11a, b, c)$$

The stress boundary condition on the free surface is written in the following form:

$$\frac{\partial u}{\partial z} = \overline{Ma} \cdot \left(\frac{\partial T^*}{\partial x} + \psi_M \cdot \frac{\partial X}{\partial x} \right) \qquad (11d)$$

with

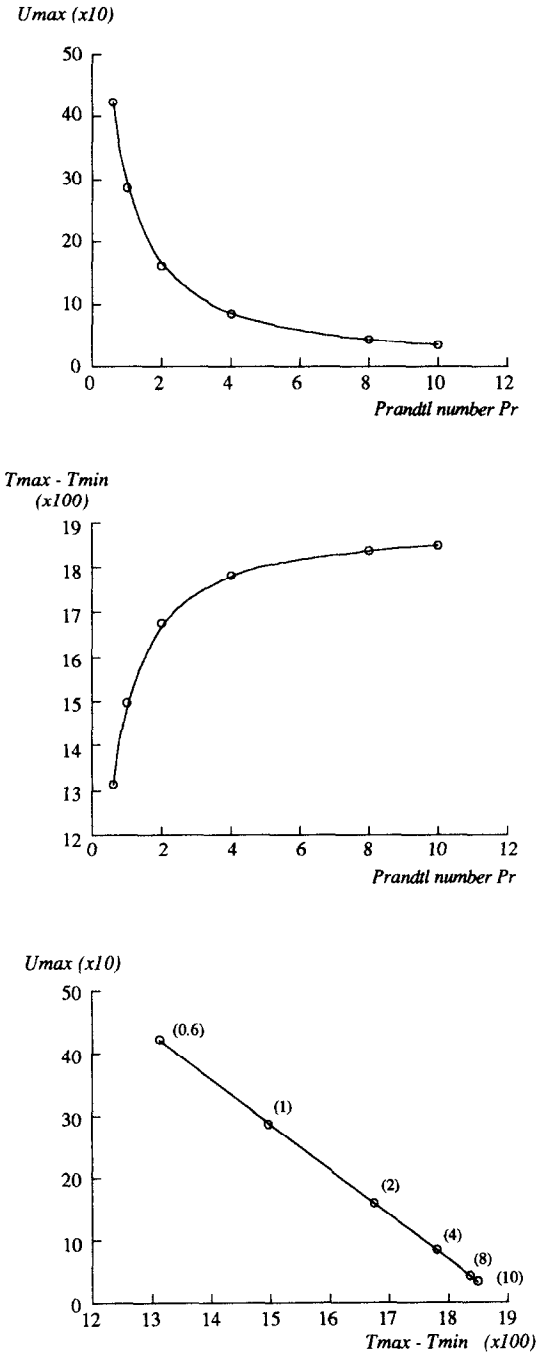

FIG. 5. Maximum of velocity and maximum of the temperature difference along the free surface as a function of the Prandtl number and maximum of velocity as a function of the maximum of the temperature difference along the free surface ($A = 4$, $Ma = 100$).

$$\overline{Ma} = Ma \cdot (1 + S_M) \quad \psi_M = \frac{Sc}{Pr} \frac{S_M}{1 + S_M}.$$

This formulation shows up that for a given geometrical configuration, the stability only depends on $(\overline{Ma}, \psi_M)$. Also, the critical values (Ma, S_M) of a bifurcation to a steady state for different choices of Sc/Pr can be deduced from the general evolution $Ma = Ma(\psi_M)$.

4.2. *Steady convection*

The flow has been computed with $Pr = 0.6$, $Sc = 60$, $Ma = 30$, $S_M = 0.03$ and for the aspect ratios $A = 3, 4, 6, 8$. Figure 10(a) shows a multiroll structure. The distortions of the isovalues of concentration (Fig. 10(c)) are those induced by the flow in the direction of the movement. The temperature field (Fig. 10(b)) is less distorted than the concentration field. This is due to the particular choice $Sc/Pr = 100$.

The S_Δ symmetry expected near the threshold for an even number of rolls is obtained for $A = 3$ and 4 with two rolls in each case. For $A = 8$, the flow structure with four rolls has lost the S_Δ symmetry. This could be the result of a secondary bifurcation. The mean dimensionless wavelength of the flow structure is equal to 3 for $A = 3$ and to 4 for $A = 4$, 6 and 8. These values are smaller than the one given at $S_M = 0.03$ by the linear theory for an infinite horizontal layer ($\lambda \approx 6.2$) [20] which would lead for example to a one-roll structure for $A = 3$ and to a two-roll structure for $A = 6$.

For an aspect ratio $A = 4$, we computed the flow for $S_M = 0.15$ and $Ma = 15$, initiating the solution with the one we obtained for $S_M = 0.03$ (Fig. 11). We still obtained a two-roll structure as for $S_M = 0.03$ and in the pure thermal case, but the S_Δ symmetry is slightly broken. As the destabilizing solutal contribution to the surface force increases with S_M, the critical Marangoni number decreases. The wavenumber of the flow structure decreases too. For $S_M > 0.1$ the linear study for an infinite horizontal layer predicts that the wavenumber becomes equal to zero [20]. This asymptotic behaviour can become clearer by noting that the thermal contribution becomes zero and that the motion is entirely controlled by the solutal gradients. Using the first order equations (equations (10), (11)) and the preponderance of the solutal contribution ($\psi_M \to \infty$), the free surface boundary conditions for the first order perturbation of concentration becomes:

$$\left[\frac{\partial u}{\partial z}\right]_{z=1} = \overline{Ma} \cdot \psi_M \cdot \left[\frac{\partial X}{\partial x}\right]_{z=1} \quad \left[\frac{\partial X}{\partial z}\right]_{z=0,1} = 0. \tag{12a, b}$$

As the conservation law of energy has no effect on the fluid motion, this problem is similar to the pure thermal situation (with T and Ma replaced by X and $\overline{Ma}\psi_M$, respectively), except for the boundary condition on the rigid bottom (see equation (12(b)). As the pure thermal problem, such a problem admits a critical value Ma_0. We can then write:

$$\overline{Ma} = \frac{Ma_0}{\psi_M} \quad \text{(in the limit } \psi_M \to \infty\text{)}. \tag{13}$$

This is the asymptotic domain where the wavenumber becomes zero. A situation can be in the asymptotic

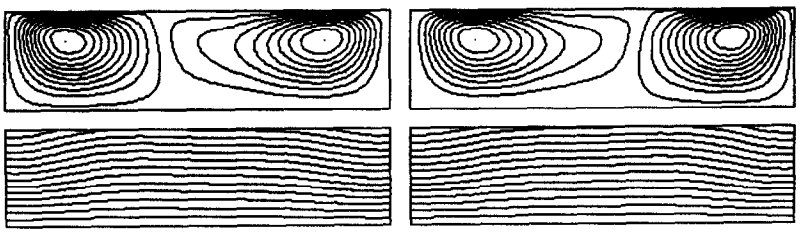

FIG. 6. Isovalues of the streamfunction (a) and isovalues of the temperature field (b) in the case $A = 4$, $Pr = 0.6$ and $Ma = 110$. Two S_A-symmetry related solutions resulting from a pitchfork bifurcation from the primary branch are obtained.

domain only if the ratio Sc/Pr is sufficiently high (S_M has then to be not too small). This is the case with $Sc/Pr = 100$ for which the wavenumber is zero above $S_M = 0.1$. The asymptotic domain corresponds to an infinite wavelength which should give rise to an expected one-roll structure we have not obtained even if we decreased the Marangoni number just above the critical value estimated about 5 for $S_M = 0.15$.

We simulated situations with $S_M = 3$ and Marangoni numbers far from the threshold ($Ma \approx 30$). For such values, the system loses the symmetry property and bifurcates to a two-roll structure (for $A = 4$) where one of the two rolls is longer than the other. In fact the length of the longer roll depends on where the perturbation of the initial state is applied on the free surface.

We computed the flow with $Pr = 0.6$, $Sc = 60$, $Ma = -30$, $S_M = -0.03$ for $A = 4$. The result is pictured in Fig. 12. In this situation, the temperature contribution to the surface force is stabilizing and the motion is due to the destabilizing solutal contribution. For such a choice of (Ma, S_M), the surface force is mainly due to the concentration gradients (Fig. 13). The velocity and the maximum of the streamfunction are smaller (see Fig. 13) than in the similar case with $Ma = 30$ and $S_M = 0.03$ given in Fig. 10 (case 2) (the

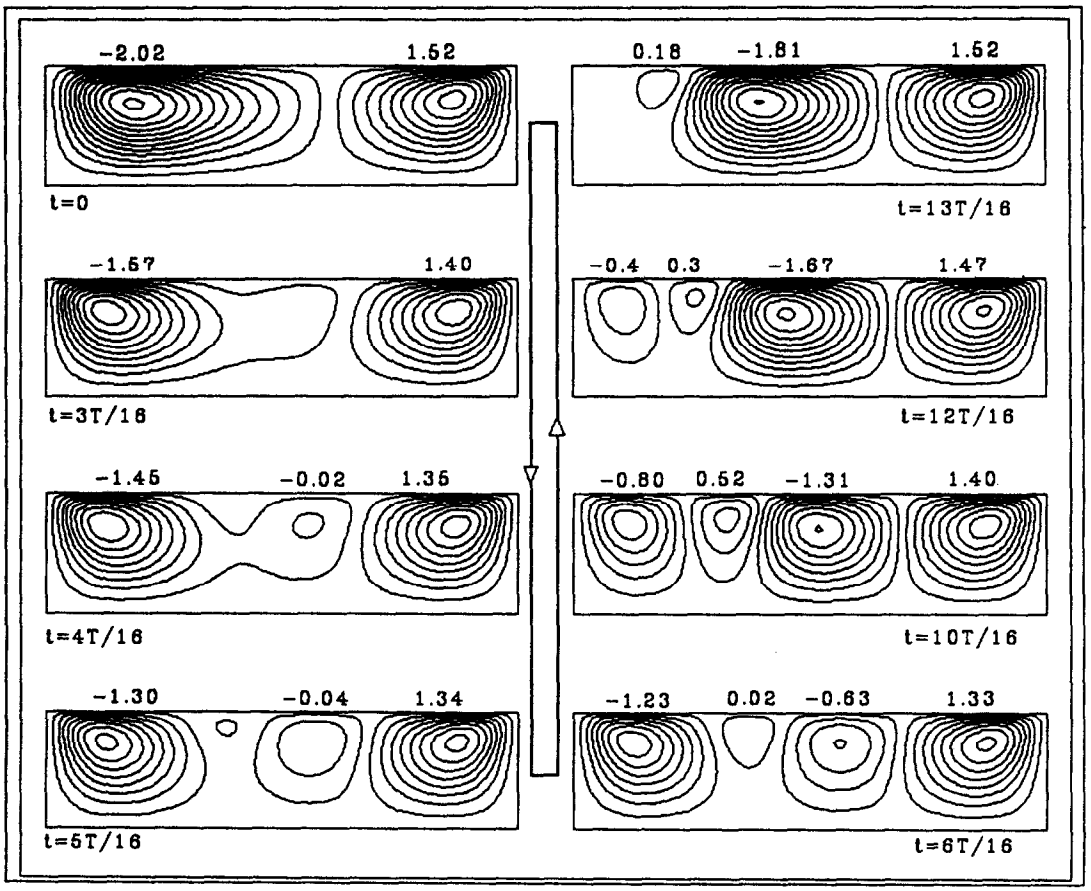

FIG. 7. Evolution of the isovalues of the streamfunction through a period $T = 1.5$ (viscous time) for $A = 4$, $Ma = 150$ and $Pr = 0.6$ (30 isovalues from -2.5 to 2.5). The maximas of the streamfunction, indicated above the cavity, are those of the corresponding roll. The instants are referred below the cavity.

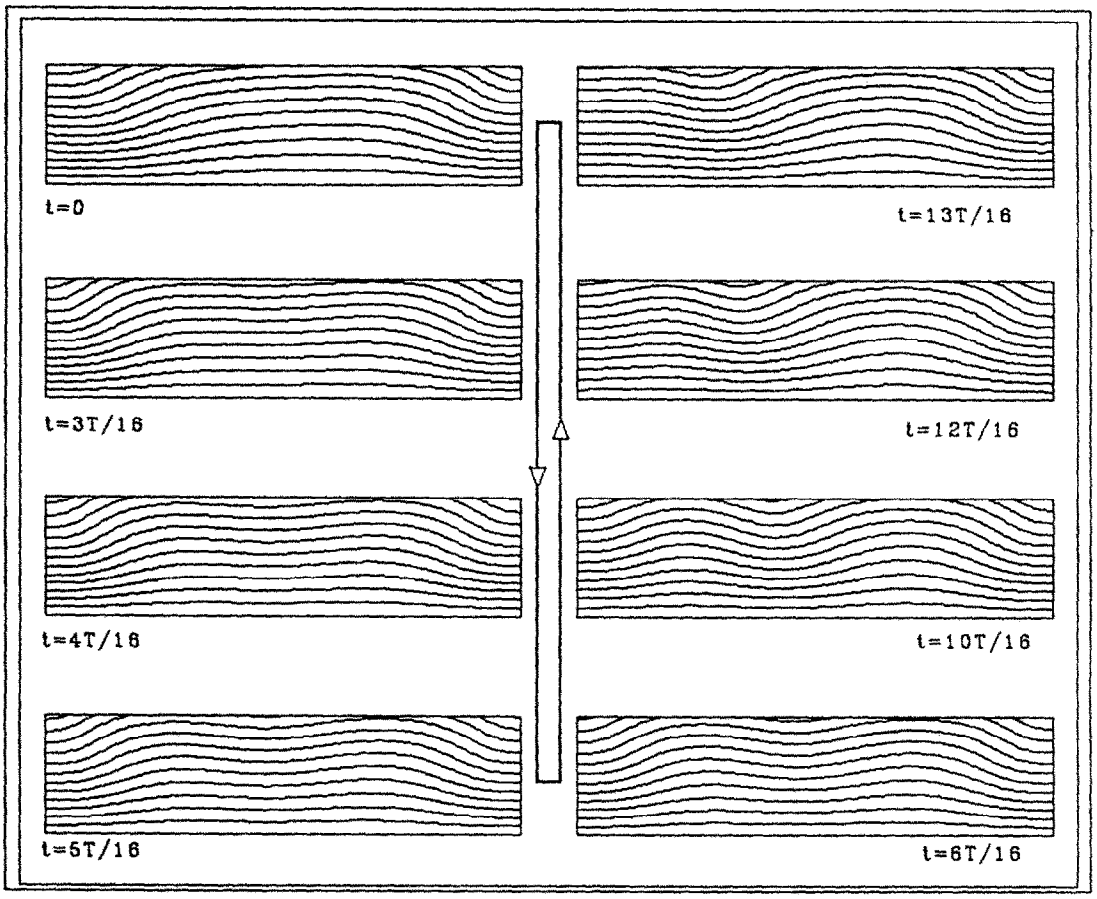

FIG. 8. Evolution of the isovalues of the temperature field through a period $T = 1.5$ (viscous time) for $A = 4$, $Ma = 150$ and $Pr = 0.6$ (10 isovalues from -0.5 to the maximum of each temperature field). The instants are referred below the cavity.

product $Ma \cdot S_M$ which drives the solutal contribution to the surface force is the same in both cases: $Ma \cdot S_M = 0.9$). These smaller values are a consequence of the stabilizing effect of the temperature. For stronger values of $|S_M|$ (belonging to the asymptotic domain), such 'corresponding' cases will be almost similar as the temperature will have no more effect on the flow.

4.3. *Time dependent convection*

Time dependent convection can be obtained as primary bifurcation for positive values of Ma and negative values of S_M. The flow has been computed with $Pr = 0.6$, $Sc = 60$, $Ma = 100$ in the cavity with $A = 4$. As the period of the oscillations decreases with increasing $|S_M|$ [20], the numerical simulation is computed with $S_M = -3$.

Initiating the flow with the solution obtained in the pure thermal case, the system evolves towards a periodic flow with a period $T = 0.808$ viscous time. The time evolution which keeps the vertical symmetry corresponds to successive transitions between the two two-roll steady configurations expected at $S_M = 0$ for $A = 4$ (Fig. 14).

For a better understanding, the physical process of the oscillatory motion with Soret effect can be first phenomenologically explained with buoyancy considerations. For such a choice of Prandtl and Schmidt numbers, the characteristic time of solutal diffusion is longer than the thermal time. Thus, the distortions of the isovalues of concentration, induced by the flow, are stronger than than those of the temperature field and the distorted field is badly restored by diffusion. As the temperature contribution is stabilizing, its distortions in the direction of the flow tend to accelerate the movement whereas the same distortions of the concentration field tend to slow it down.

When the isovalues of temperature are distorted in the direction of the flow, they speed the process up. If we suppose that, at this moment, there is no deformation of the concentration field, the flow intensity becomes stronger. But, in the same time, the distortions of the concentration, which have a stabilizing effect on the fluid motion, are gradually dragged by the flow. As soon as the two fields are distorted in the direction of the flow, the velocity decreases under the stabilizing effect of the concentration, until the rotation sense of the motion is inverted. During this process, the distortions of the isovalues begin to decrease following the decrease of the flow intensity,

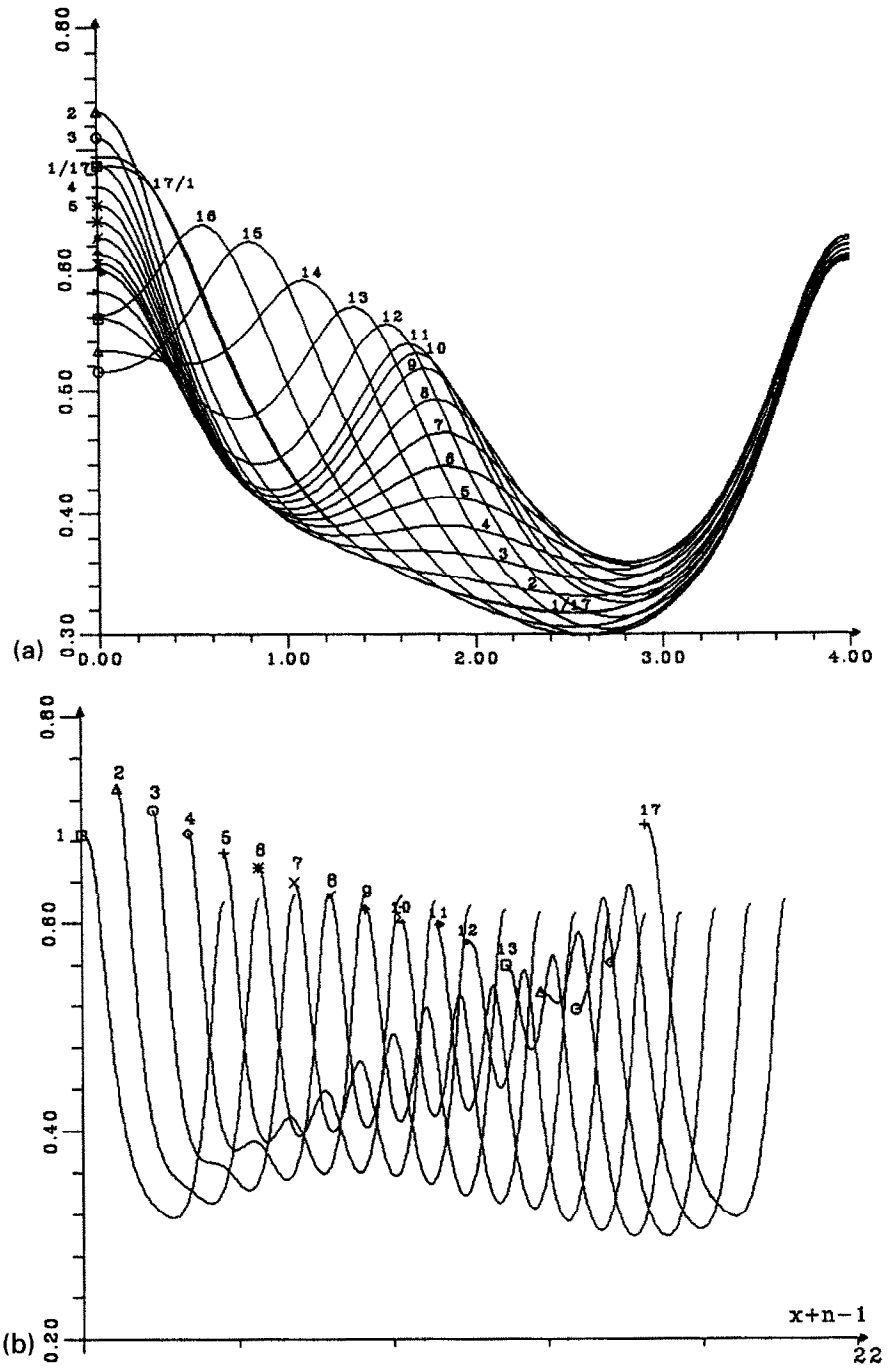

FIG. 9. (a) Evolution of the temperature profile on the free surface for $Pr = 0.6$, $A = 4$ and $Ma = 150$ through a period T (16 records separated by a time $\Delta t = T/16$ describe a period). (b) Same evolution as for (a) but each of the fields is translated along the x axis with one unit on the right.

particularly for the temperature field well restored by diffusion. Thus, as the rotation sense of the motion is inverted, the isovalues of the temperature are soon distorted in the direction of the flow whereas the isovalues of concentration are still distorted in the previous direction of the flow. The two contributions act in the same way and tend to increase the fluid motion. The distortions of the isovalues of the concentration are gradually induced in the direction of the flow and half a period is then described.

In the case with free surface, Fig. 14 shows that the change of the direction of rotation occurs through the appearance of two contrarotative rolls which grow until they replace the initial ones. In such case, the flow is driven by surface tension forces created by gradients due to the distortions of the isovalues near

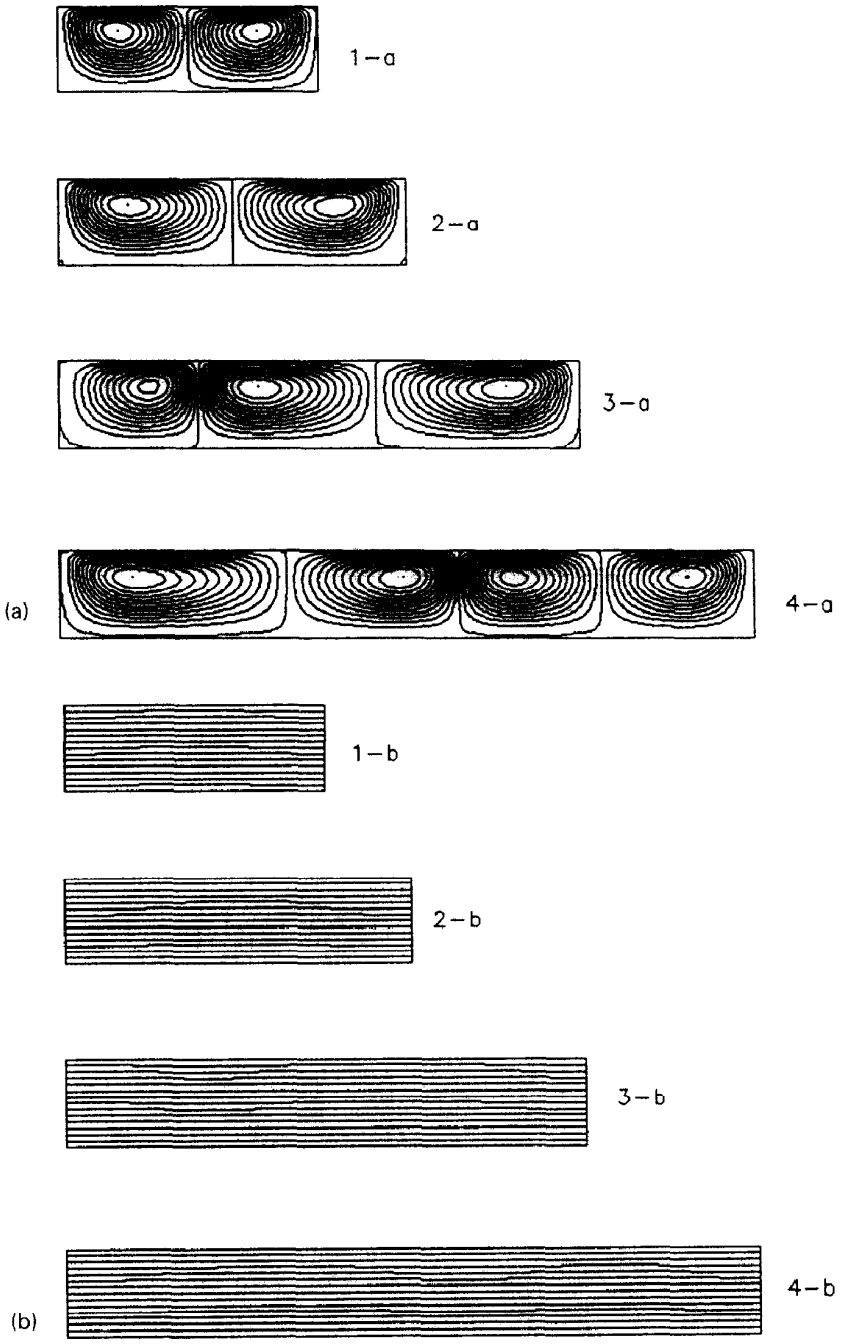

FIG. 10. Isovalues of the streamfunction (a), the temperature (b) and the concentration (c) fields with $Ma = 30$, $S_M = 0.03$, $Pr = 0.6$ and $Sc = 60$ (25 isovalues are plotted between the minimum and the maximum of each configuration for the streamfunction and the concentration, 15 for the temperature) for the aspect ratios: (1) $A = 3$, (2) $A = 4$, (3) $A = 6$, (4) $A = 8$.

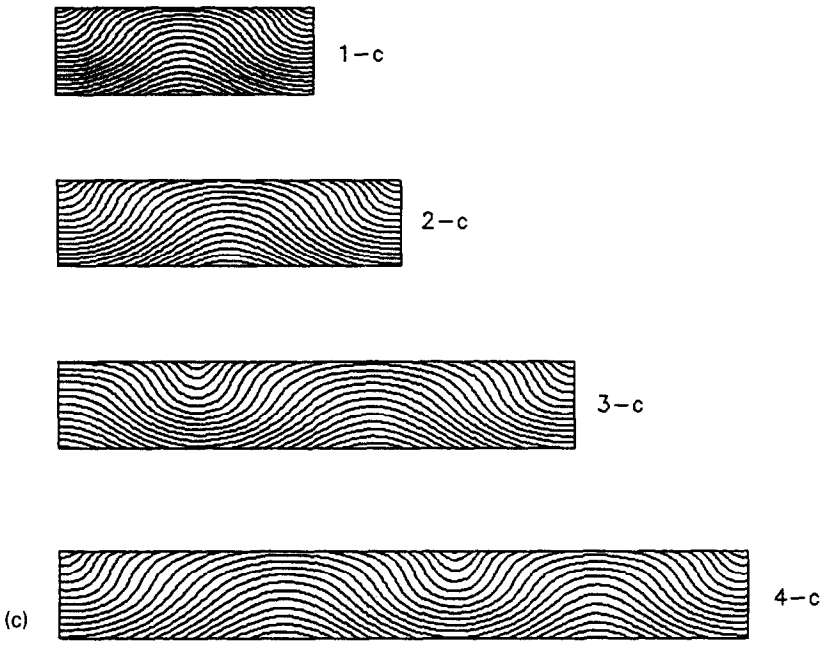

FIG. 10.—*continued.*

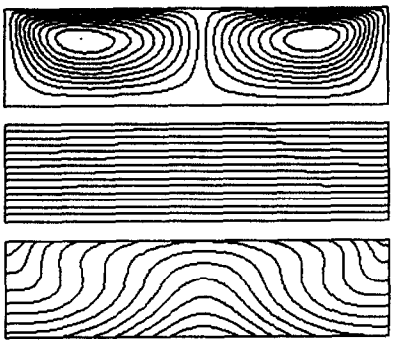

FIG. 11. Isovalues of the streamfunction, the temperature and the concentration fields for $A = 4$, $Pr = 0.6$, $Sc = 60$, $Ma = 15$, $S_M = 0.15$ (20 isovalues between the minimum and the maximum are plotted for the streamfunction, 15 for the temperature and the concentration).

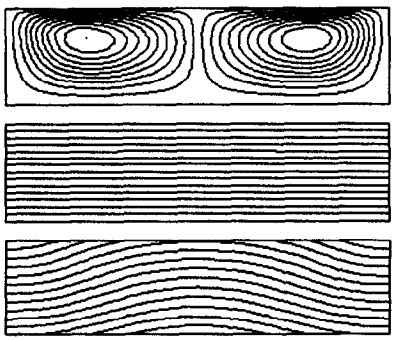

FIG. 12. Isovalues of the streamfunction, of the temperature and the concentration fields for $A = 4$, $Pr = 0.6$, $Sc = 60$, $Ma = -30$, $S_M = -0.03$ (20 isovalues between the minimum and the maximum are plotted for the streamfunction, 15 for the temperature and the concentration).

the free surface. These distortions (particularly those of the concentration field which are first responsible for the inversion of the flow) occur first in the zone where the flow goes down after having been accelerated along the free surface. The new rolls are then generated locally in these places and they gradually grow following the displacement of the concentration distortions across the cavity (travelling wave behaviour depicted in Figs. 15(a) and (b). Due to the change of the direction of rotation, the new pair appears alternatively in the center and in the corners of the cavity (Fig. 14).

Figure 15(c) tries to depict the inversion of the flow in the left half part of the cavity. At step 1, T and c are still distorted in the previous direction of the flow (anti-clockwise roll of step 9). Thus the stabilizing thermal contribution to the surface force (1-T) tends to accelerate the flow in this direction whereas the destabilizing solutal contribution (1-c) opposes the movement and creates a new contrarotative roll in this left part of the cavity. At step 2, the new clockwise roll has settled. It already induces temperature distortions in such a way that the temperature gradients now drive the new flow (2-T) as well as the concentration gradients (2-c). At step 3, the clockwise roll is stronger. The favourable thermal contribution has increased (3-T), but the concentration field is now affected by the clockwise roll and generate concentration gradients (near $x = 2$) opposed to the motion (3-c). This solutal contribution will increase and generate at step 4 a global contribution opposed to the movement near $x = 2$ (Fig. 15(b)). This corresponds to the initiation of a new contrarotative roll near $x = 2$.

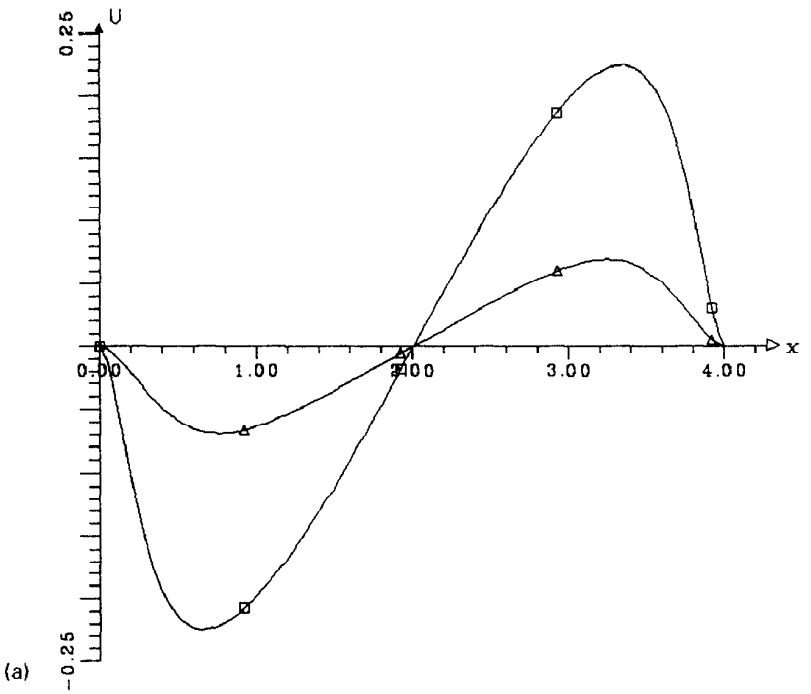

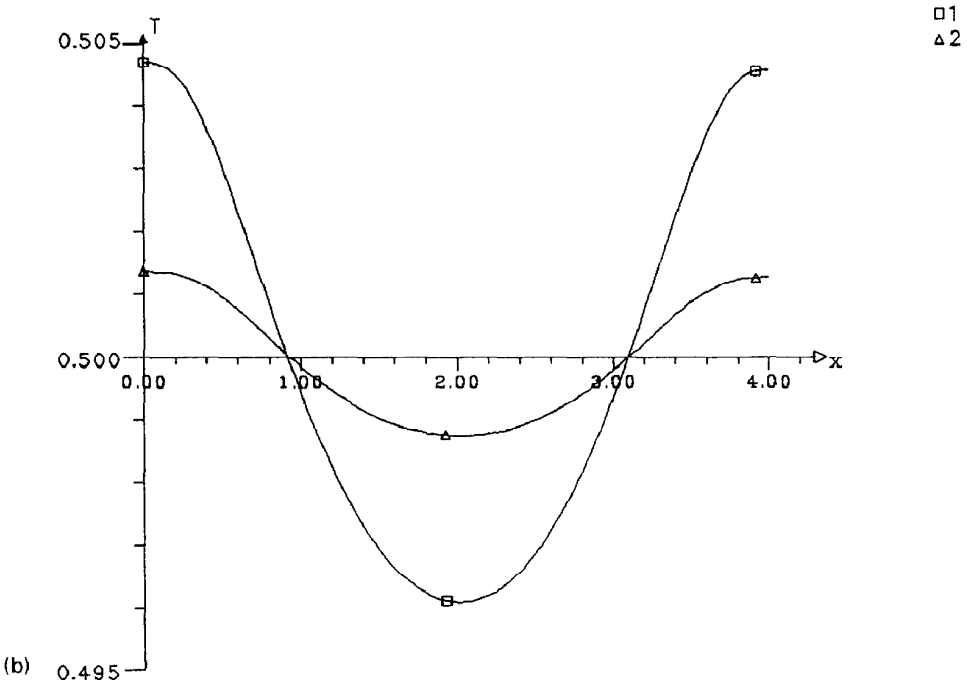

FIG. 13. Velocity (a), temperature (b) and concentration (c) profiles along the free surface with $A = 4$, $Pr = 0.6$, $Sc = 60$ for the two situations (1), $(Ma, S_M) = (30, 0.03)$ and (2), $(Ma, S_M) = (-30, -0.03)$.

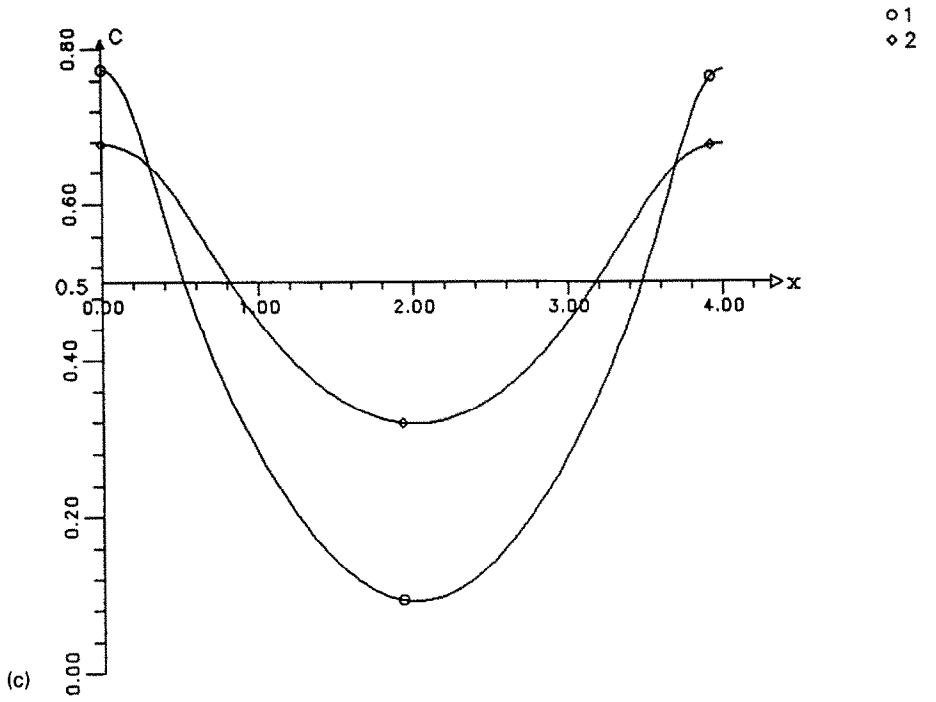

FIG. 13.—*continued.*

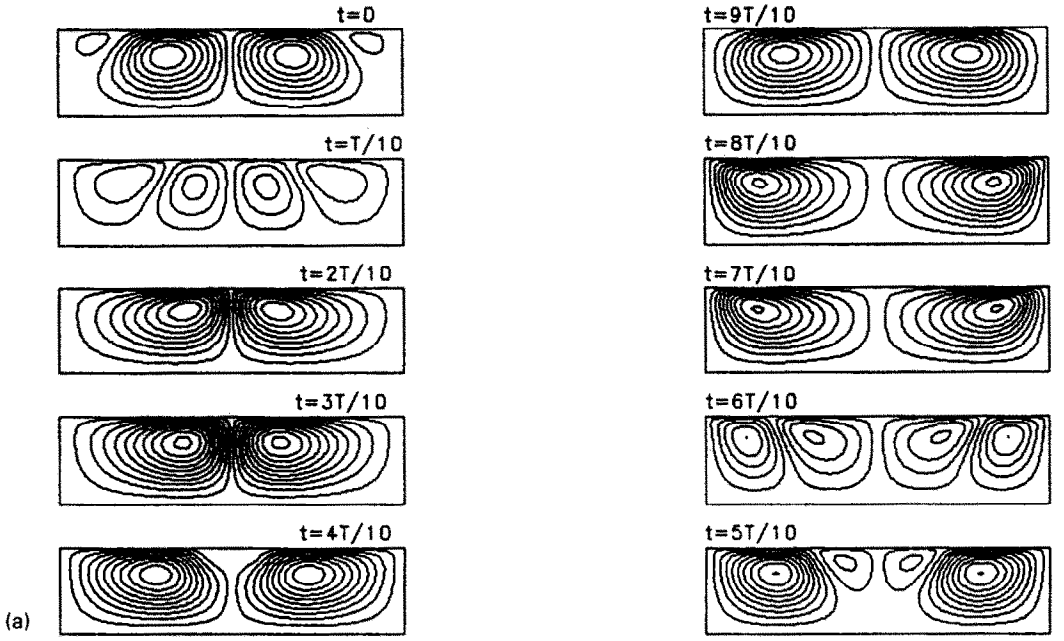

FIG. 14. Time evolution of the isovalues of the streamfunction (a), temperature (b) and concentration (c) fields through a period T for the time-dependent situation corresponding to a primary bifurcation for $A = 4$, $Pr = 0.6$, $Sc = 60$, $Ma = 100$, $S_M = -3$. The plots correspond to successive times $t = n \cdot T/10$ with $0 \leqslant n \leqslant 9$ (20 isovalues between -0.5 and 0.5 for the streamfunction, 15 between -0.5 and 0.7 for the temperature and 11 between -0.5 and 0.5 for the concentration.

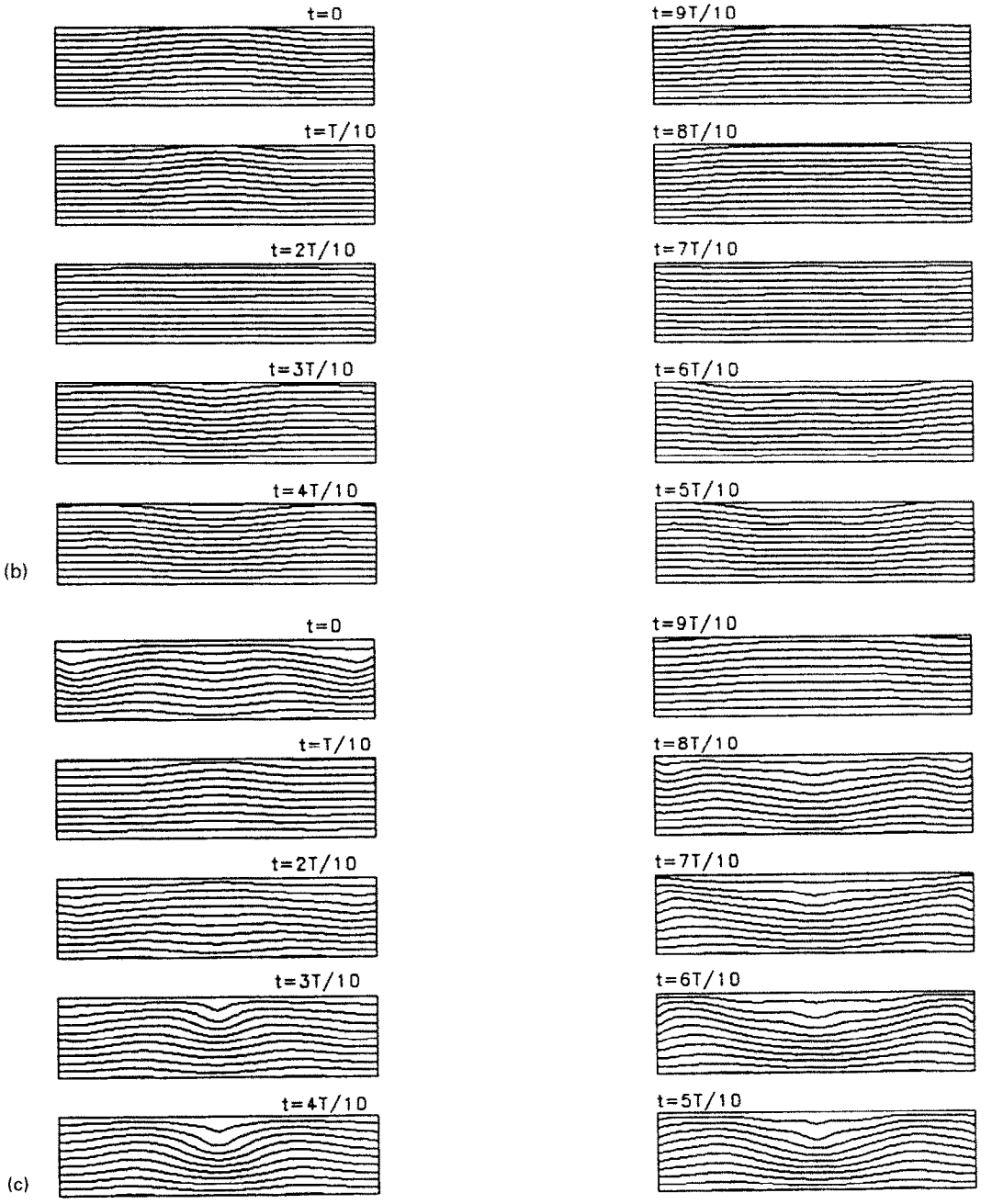

FIG. 14.—*continued.*

5. CONCLUSION

Marangoni instability has been studied numerically in a two dimensional bounded cavity for which the free surface is assumed to be plane. In the case of a one-component fluid, the symmetry properties have been discussed and a good agreement with the theory has been pointed out. The influence of the Prandtl number on the flow intensity has been investigated for a cavity with an aspect ratio $A = 4$ and a fixed Marangoni number $Ma = 100$. We exhibited a linear dependence of the maximum velocity on the free surface with the maximum temperature difference along the free surface. In the case $A = 4$, $Pr = 0.6$, a further increase of the Marangoni number leads first to a secondary steady bifurcation with breaking of

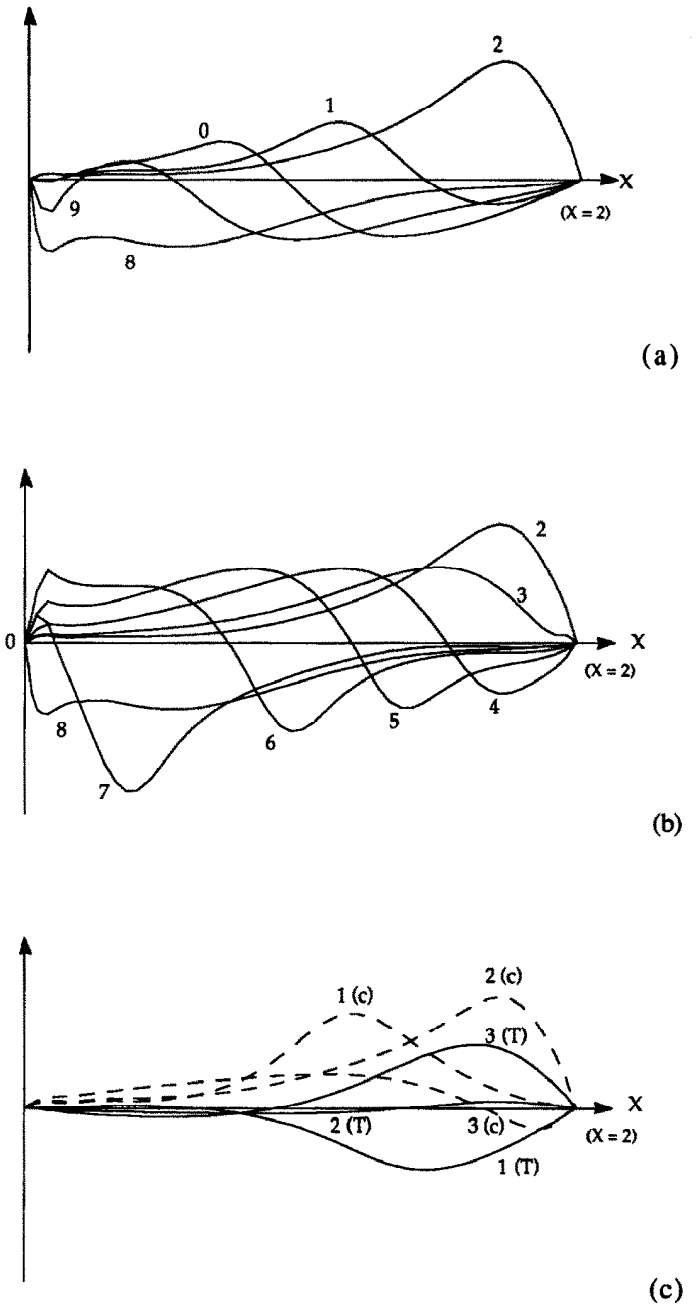

FIG. 15. The two upper curves (a) and (b) describe the time evolution of the surface force $\partial u/\partial z$ along half the free surface (from $x = 0$ to 2) through a period T (the numbers (n) refer to the situations plotted in Fig. 14 ($t = n \cdot T/10$)). The travelling wave characteristic of the two transitions is thus pictured. The curve (c) describes the time evolution of the thermal and solutal contributions to the surface force, respectively, $Ma \cdot Pr^{-1} \cdot \partial T/\partial x$ and $Ma \cdot Pr^{-1} \cdot S_M \cdot \partial c/\partial x$ through the records 1, 2 and 3. The creation of a new roll near $x = 2$ is thus depicted.

symmetry, and then to a Hopf bifurcation giving rise to oscillatory motions which have been computed through a period for $Ma = 150$.

In the case of a binary mixture subjected to Soret effect, direct simulations are compared to the structures expected by the linear theory. The flow behaviours (steady or time dependent) correspond to those expected, but the wavelengths in steady situations are smaller. For most of the steady situations we computed, the system loses the symmetry property. This can be related to secondary bifurcations which occur close to the onset. Asymptotic behaviours (corresponding to the preponderance of the solutal contribution) are discussed in a more general dimen-

sionless form than the one generally used in this problem. When the thermal contribution to the surface force has a destabilizing effect on the fluid motion and the solutal contribution has a stabilizing effect, oscillatory motions are predicted as primary bifurcation and have effectively been obtained. Such behaviours are well explained in terms of competition between thermal and solutal forces.

Acknowledgement—The authors are indebted to Professor J. C. Legros and Doctor S. Van Vaerenbergh from the Microgravity Research Center of the Université Libre de Bruxelles, to Doctor B. Roux from the Institut de Mécanique des Fluides of Marseille and to Doctor L. Tuckerman from the University of Austin for fruitful discussions. The present work was conducted within the frame of the CNES microgravity program. Computations were carried out on a Cray-2 computer with the support of the Centre de Calcul Vectoriel pour la Recherche (CCVR).

REFERENCES

1. J. R. A. Pearson, On convection cells induced by surface tension, *J. Fluid Mech.* **4,** 489–500 (1958).
2. D. A. Nield, Surface tension and buoyancy effects in cellular convection, *J. Fluid Mech.* **19,** 341–352 (1964).
3. S. H. Davis, Buoyancy–surface tension instability by the method of energy, *J. Fluid Mech.* **39,** 347–359 (1969).
4. J. W. Scanlon and L. A. Segel, Finite amplitude cellular convection induced by surface tension, *J. Fluid Mech.* **30,** 149–162 (1967).
5. A. Cloot and G. Lebon, A non-linear stability analysis of the Bénard–Marangoni problem, *J. Fluid Mech.* **145,** 447–469 (1984).
6. L. E. Scriven and C. V. Sternling, On cellular convection driven by surface-tension gradients: effect of mean surface tension and surface viscosity, *J. Fluid Mech.* **19,** 321–340 (1964).
7. K. A. Smith, On convective instability induced by surface tension, *J. Fluid Mech.* **24,** 401–414 (1966).
8. D. A. Goussis and R. E. Kelly, On the thermocapillary instabilities in a liquid layer heated from below, *Int. J. Heat Mass Transfer* **33,** 2237–2245 (1990).
9. S. H. Davis and G. M. Homsy, Energy stability theory for free-surface problems: buoyancy–thermocapillary layers, *J. Fluid Mech.* **98,** 527–553 (1980).
10. J. L. Castillo and M. G. Velarde, Buoyancy–thermocapillary instability: the role of interfacial deformation in one- and two-component fluid layers heated from below or above, *J. Fluid Mech.* **125,** 463–474 (1982).
11. S. Rosenblat, S. H. Davis and G. M. Homsy, Nonlinear Marangoni convection in bounded layers, *J. Fluid Mech.* **120,** 91–138 (1982).
12. A. I. Van de Vooren and H. A. Dijkstra, A finite element stability analysis for the Marangoni problem in a rectangular container with rigid sidewalls, *Comput. Fluids* **17,** 467–485 (1989).
13. H. A. Dijkstra, On the structure of cellular solutions in Rayleigh–Bénard–Marangoni flows in small-aspect-ratio containers, *J. Fluid Mech.* **243,** 73–102 (1992).
14. S. R. De Groot and P. Mazur, *Non-Equilibrium Thermodynamics*. North-Holland, Amsterdam (1969).
15. E. Knobloch, Convection in binary fluids, *Phys. Fluids* **23,** 1918–1920 (1980).
16. D. A. Nield, The thermohaline Rayleigh–Jeffreys problem, *J. Fluid Mech.* **29,** 545–558 (1967).
17. D. T. J. Hurle and E. Jakeman, Soret driven thermosolutal convection, *J. Fluid Mech.* **47,** 667–687 (1971).
18. E. Knobloch and D. R. Moore, Linear stability of experimental Soret convection, *Phys. Rev. A* **37,** 860–870 (1988).
19. J. L. Castillo and M. G. Velarde, Thermal diffusion and the Marangoni–Bénard instability of a two component fluid layer heated from below, *Phys. Letters A* **66,** 489–491 (1978).
20. S. Van Vaerenbergh, P. Colinet, Ph. Georis and J. C. Legros, Preparatory results for a Marangoni–Bénard experiment with Soret effect under microgravity conditions. In *Reviewed Proceedings of the First International Symposium on Hydromechanics and Heat and Mass Transfer in Microgravity, Perm-Moscow, Russia*. Gordon and Breach, New York (1991).
21. H. Benhadid, Etude numerique des mouvements convectifs au sein des fluides à faible nombre de Prandtl. Application à l'élaboration des cristaux métalliques et semi-conducteurs, Doctorate Thesis, Université d'Aix-Marseille II (1989).
22. K. H. Winters, Th. Plesser and K. A. Cliffe, The onset of convection in a finite container due to surface tension and buoyancy, *Physica D* **29,** 387–401 (1988).